

# GRAVMAD: GROUNDED SPATIAL VALUE MAPS GUIDED ACTION DIFFUSION FOR GENERALIZED 3D MANIPULATION

Yangtao Chen<sup>1\*</sup>, Zixuan Chen<sup>1\*</sup>, Junhui Yin<sup>1</sup>, Jing Huo<sup>1†</sup>, Pinzhuo Tian<sup>3</sup>, Jieqi Shi<sup>2</sup>, Yang Gao<sup>1,2</sup>

<sup>1</sup>State Key Laboratory for Novel Software Technology, Nanjing University, Nanjing, China  
502023330009@smail.nju.edu.cn, {chenzx, huojing, gaoy}@nju.edu.cn,  
yinjunhui@smail.nju.edu.cn

<sup>2</sup>School of Intelligence Science and Technology, Nanjing University (Suzhou Campus), Nanjing, China  
jayceesjq@gmail.com

<sup>3</sup>School of Computer Engineering and Science, Shanghai University, Shanghai, China  
pinzhuo@shu.edu.cn

## ABSTRACT

Robots’ ability to follow language instructions and execute diverse 3D tasks is vital in robot learning. Traditional imitation learning-based methods perform well on seen tasks but struggle with novel, unseen ones due to variability. Recent approaches leverage large foundation models to assist in understanding novel tasks, thereby mitigating this issue. However, these methods lack a task-specific learning process, which is essential for an accurate understanding of 3D environments, often leading to execution failures. In this paper, we introduce **GravMAD**, a sub-goal-driven, language-conditioned action diffusion framework that combines the strengths of imitation learning and foundation models. Our approach breaks tasks into sub-goals based on language instructions, allowing auxiliary guidance during both training and inference. During training, we introduce **Sub-goal Keypose Discovery** to identify key sub-goals from demonstrations. Inference differs from training, as there are no demonstrations available, so we use pre-trained foundation models to bridge the gap and identify sub-goals for the current task. In both phases, **GravMaps** are generated from sub-goals, providing flexible 3D spatial guidance compared to fixed 3D positions. Empirical evaluations on RLBench show that GravMAD significantly outperforms state-of-the-art methods, with a 28.63% improvement on novel tasks and a 13.36% gain on tasks encountered during training. These results demonstrate GravMAD’s strong multi-task learning and generalization in 3D manipulation. Video demonstrations are available at: <https://gravmad.github.io>.

## 1 INTRODUCTION

One of the ultimate goals of general-purpose robot manipulation learning is to enable robots to perform a wide range of tasks in real-world 3D environments based on natural language instructions (Hu et al., 2023a). To achieve this, robots must understand task language instructions and align them with the spatial properties of relevant objects in the scene. Additionally, robots must effectively generalize across different tasks and environments; otherwise, their practical application will be limited Zhou et al. (2023). For example, if a robot has learned the policy for the task “*Take the chicken off the grill*”, it should also be able to perform the task “*Put the chicken on the grill*”. Without this generalization ability, its utility will be greatly reduced. Recent research in robot learning for 3D manipulation tasks has focused on two mainstream approaches: imitation learning-based methods and pre-trained foundation model-based methods. Imitation learning-based methods learn end-to-end policies from expert demonstrations in attempt to address 3D manipulation tasks (Walke et al., 2023; Padalkar et al., 2024; Argall et al., 2009). By designing various learning frameworks, such as incorporating

\*Equal contribution.

†Corresponding author.

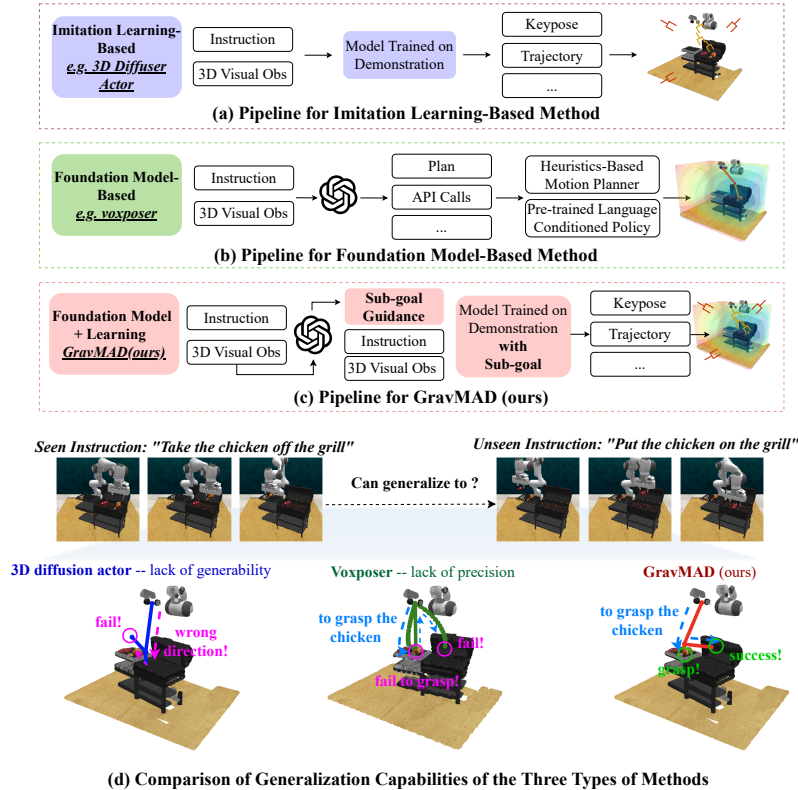


Figure 1: **Comparison of Pipelines.** (a) Imitation learning-based methods learn end-to-end policies that map language and 3D observations to actions for precise manipulation. (b) Foundation models-based methods use LLMs/VLMs to process inputs, generate plans, and execute actions with predefined primitives for task generalization. (c)(d) GravMAD combines both, using sub-goal guidance to leverage the language understanding of foundation models and the policy learning of imitation learning for precise and generalized manipulation.

different 3D representations (Shridhar et al., 2023; Chen et al., 2023; Goyal et al., 2023), policy representations (Ze et al., 2024; Ke et al., 2024; Yan et al., 2024), and multi-stage architectures (Gervet et al., 2023; Goyal et al., 2024), imitation learning-based policies can map perceptual information and language instructions to actions that complete complex 3D manipulation tasks. However, these policies often overfit to specific tasks (Xie et al., 2024; Zhang et al., 2024), leading to significant performance degradation or even failure when applied to tasks that differ from those encountered during training (Brohan et al., 2023a; Zitkovich et al., 2023).

Another line of cutting-edge research seeks to leverage foundation models trained on internet-scale data (OpenAI, 2023; Yang et al., 2023b) to enhance policy generalization across a variety of tasks (Brohan et al., 2023b; Hu et al., 2023b; Huang et al., 2023). Unlike traditional imitation learning-based methods, approaches using pre-trained foundation models typically decouple perception, reasoning, and control during manipulation (Sharan et al., 2024). However, this decoupling often leads to a limited understanding of scenes and manipulation tasks (Huang et al., 2024), allowing robots to conceptually grasp tasks but failing to accurately complete tasks in 3D environments, resulting in failures. This underscores a key challenge: both imitation learning-based and foundation model-based approaches struggle to balance precision and generalization when adapting to novel 3D manipulation tasks. Such a challenge raises a crucial question: *Can the strengths of both approaches be combined to achieve precise yet generalized 3D manipulation?*

To this end, we propose discovering key sub-goals for 3D manipulation tasks as a bridge between foundation models and learned policies, leading to the development of **Grounded Spatial Value Maps-guided Action Diffusion (GravMAD)**, a novel sub-goals-driven, language-conditioned action diffusion framework. Specifically, a new data distillation method called **Sub-goal Keypose Discovery** is introduced during the training phase. This method identifies the key sub-goals required for each

sub-task stage from the demonstrations. In the inference phase, pre-trained foundation models are leveraged to interpret the robot’s 3D visual observations and task language instructions, directly identifying task sub-goals. Once the task sub-goals are obtained, the voxel value maps introduced in Voxposer (Huang et al., 2023) are used to generate the corresponding **Grounded Spatial Value Maps (GravMaps)**. These maps reflect both the cost associated with each sub-goal and the ideal gripper openness. The closer to the sub-goal, the lower (cooler) the cost; the farther away, the higher (warmer) the cost, while also indicating the gripper’s state within the sub-goal range. Thus, they serve as intuitive tools for grounding language instructions into 3D robotic workspaces. Finally, the generated GravMaps are integrated with the policy diffusion architecture proposed in 3D diffuser actor (Ke et al., 2024), forming the GravMAD framework. This enables the robot to utilize 3D visual observations, task language instructions, and GravMaps guidance to denoise random noise into precise end-effector poses. As shown in Fig. 1, GravMAD effectively combines the precise manipulation capabilities of imitation learning-based methods with the reasoning and generalization abilities of foundation model-based approaches. We extensively evaluate GravMAD on RL Bench (James et al., 2020a), a representative benchmark for instruction-following 3D manipulation tasks. The results show that GravMAD not only performs well on tasks encountered during training but also significantly outperforms state-of-the-art baseline methods in terms of generalization to novel tasks.

In summary, our contributions are: **1)** We propose the concept of discovering key sub-goals in 3D manipulation tasks to bridge the gap between foundation models and learned policies. In the training phase, we introduce a data distillation method, **Sub-goal Keypose Discovery**, to identify task sub-goals. In the inference phase, foundation models are used for this purpose. **2)** We generate **GravMaps** from these sub-goals, translating task language instructions into 3D spatial sub-goals and reflecting spatial relationships in the environment. **3)** We propose a new action diffusion framework, **GravMAD**, guided by GravMaps. It is sub-goal-driven and language-conditioned, combining the precision of imitation learning with the generalization capabilities of foundation models. **4)** We design two types of tasks on RL Bench: 12 base tasks directly selected from RL Bench and 8 novel tasks with modified scene configurations or task instructions. GravMAD achieves at least **13.36%** higher success rates than state-of-the-art baselines on the 12 base tasks encountered during training, and surpasses them by **28.63%** on the 8 novel tasks, highlighting its strong generalization capabilities.

## 2 RELATED WORKS

**Learning 3D Manipulation Policies from Demonstrations.** Recent works have employed various perception methods to learn 3D manipulation policies from demonstrations to tackle the complexity of reasoning in 3D space. These methods include using 2D images (Brohan et al., 2023a; Zitkovich et al., 2023; Jang et al., 2022), voxels (Shridhar et al., 2023; James et al., 2022), point clouds (Chen et al., 2023; Yuan et al., 2023), multi-view virtual images (Goyal et al., 2023; 2024), and feature fields (Gervet et al., 2023). To support policy learning, some studies (Ke et al., 2024; Xian et al., 2023; Yan et al., 2024; Ze et al., 2024) have integrated 3D scene representations with diffusion models (Ho et al., 2020). These approaches attempt to handle the multi-modality of actions, in contrast to behavior cloning methods that train deterministic policies. By leveraging 3D representation learning, these policies can accurately complete tasks by accounting for the spatial properties of objects, such as orientation and position. This is especially effective for tasks that closely resemble those encountered during training Ze et al. (2023). However, these policies often lack the language understanding and generalization abilities of foundation models. Our method extends the diffusion architecture (Ke et al., 2024) to fully leverage demonstration data and enhances policy generalization by integrating foundation models, combining the strengths of both approaches.

**Foundation Models for 3D Manipulation.** Recent foundation models trained on internet-scale data have shown strong zero-shot and few-shot generalization, offering new opportunities for complex 3D manipulation tasks (Hu et al., 2023a; Zhou et al., 2023). While some approaches fine-tune vision-language models with embodied data (Driess et al., 2023; Li et al., 2024), this increases computational costs due to the large data requirements. Alternatively, foundational vision models can generate visual representations for 3D tasks (Zhang et al., 2024; 2023), but they often lack the reasoning capabilities needed for complex tasks. To address these challenges, some studies leverage large language models (LLMs) as high-level planners (Brohan et al., 2023b; Hu et al., 2023b; Huang et al., 2022), generating language-based plans executed by lower-level policies. Others utilize LLMs’ code-writing abilities to control robots via API calls or to create value maps for planning robot

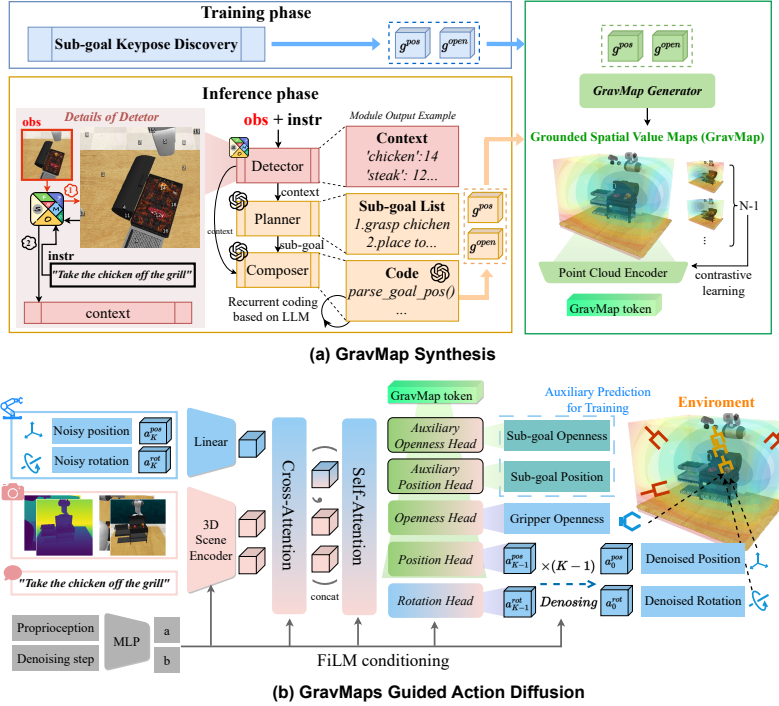


Figure 2: **GravMAD Overview.** (a) **GravMap Synthesis:** During training, we use Sub-goal Keypose Discovery to obtain sub-goals  $g^{\text{pos}}$  and  $g^{\text{open}}$ . During inference, the Detector, Planner, and Composer pipeline interprets visual observations and language instructions to derive  $g^{\text{pos}}$  and  $g^{\text{open}}$ , which are processed into a GravMap and encoded as a GravMap token. (b) **GravMaps Guided Action Diffusion:** The policy network perceives the scene and denoises noisy actions guided by the GravMap token. After  $K$  denoising steps, the clean actions are executed by the robot.

trajectories (Liang et al., 2023; Huang et al., 2023). However, these methods often sacrifice precision due to a rough understanding of complex 3D scenes. Recent works have combined the reasoning capabilities of foundation models with fine-grained control in 3D manipulation to overcome this limitation (Huang et al., 2024; Sharan et al., 2024). For example, Huang et al. (2024) uses pre-trained vision-language models (VLMs) to provide spatial constraints and a nonlinear solver to generate precise grasp poses. Our method combines the learning power of diffusion architectures with the generalization of VLMs. VLMs generate spatial value maps that guide action diffusion, enabling precise control and multi-task generalization in 3D manipulation tasks.

### 3 METHOD

In this section, we introduce **GravMAD** (Grounded Spatial Value Maps Guided Action Diffusion), a multi-task, sub-goal-driven, language-conditioned diffusion framework for 3D manipulation, as shown in Fig. 2. We divide GravMAD’s design into three parts: Section 3.1 defines the 3D manipulation problem, Section 3.2 explains the definition and generation of GravMaps, and Section 3.3 details how GravMaps guide action diffusion in 3D manipulation.

#### 3.1 PROBLEM FORMULATION

We consider a problem setting where expert demonstrations consist of a robot trajectory  $(o_1, a_1, o_2, a_2, \dots)$  and a natural language instruction  $\ell \in \mathcal{L}$  that describes the task goal. Each observation  $o_t \in \mathcal{O}$  includes RGB-D images from one or more viewpoints. Each action  $a_t \in \mathcal{A}$  contains the 3D position of the robot’s end-effector  $a^{\text{pos}} \in \mathbb{R}^3$ , a 6D rotation  $a^{\text{rot}} \in \mathbb{R}^6$ , and a binary gripper state  $a^{\text{open}} \in \{0, 1\}$ . To avoid quaternion discontinuities, we use the 6D rotation representation (Ke et al., 2024). In this setting, we assume that a robotic task is composed of multiple sub-tasks, with each sub-task completed when the robot reaches a sub-goal  $g_t \in \mathcal{G}$ , which specifies

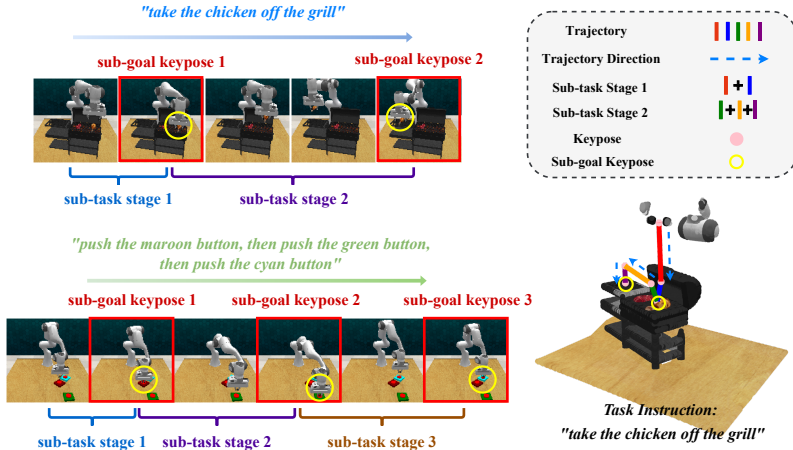


Figure 3: Visualization of sub-goal keyposes and sub-task stages. The left sub-figure shows image-based sub-goal keyposes and sub-task stages for “take the chicken off the grill” and “push the \_\_\_ button” tasks. The right shows the sub-goal key poses and sub-task stages in the trajectory for the “take the chicken off the grill” task.

the 3D position  $g^{\text{pos}} \in \mathbb{R}^3$ , the gripper openness  $g^{\text{open}} \in \{0, 1\}$ , and the 6D rotation  $g^{\text{rot}} \in \mathbb{R}^6$ . Based on this, we construct a new dataset  $\mathcal{D} = \{\zeta_1, \zeta_2, \dots\}$  from expert demonstrations. Each demonstration  $\zeta$  consists of trajectories with sub-goals  $\{(o_1, g_1, a_1), (o_2, g_2, a_2), \dots\}$  and the corresponding language instruction  $\ell$ . Our goal is to learn a policy  $\pi : (\mathcal{O}, \mathcal{L}, \mathcal{G}) \mapsto \mathcal{A}$ , which maps observations  $o_t$ , sub-goals  $g_t$ , and instructions  $\ell$  to actions  $a_t$ . To facilitate sub-task segmentation and efficiently learn the policy, we frame the robot’s 3D manipulation learning problem as a keypose prediction problem following prior works (James & Davison, 2022; James et al., 2022; Goyal et al., 2023; Shridhar et al., 2023). Our model progressively predicts the next keypose based on current observations and uses a sampling-based motion planner (Klemm et al., 2015) to plan the trajectory between two keyposes. In the existing keypose discovery method (James & Davison, 2022), a pose is identified as a keypose when the robot’s joint velocities are near zero, and the gripper state remains unchanged. Our work filters the task’s sub-goals based on these keyposes to facilitate sub-task segmentation and ensure efficient completion of the overall task.

### 3.2 GRAVMAP: GROUNDED SPATIAL VALUE MAPS

To tackle generalization challenges in 3D manipulation tasks, we introduce the spatial value maps (**GravMap**), an adaptation of the voxel value maps proposed by Huang et al., denoted as  $m$ . GravMaps are adaptively synthesized based on task variations, translating language instructions into 3D spatial sub-goals and reflecting the spatial relationships within the environment. This provides precise guidance for robotic action diffusion. Each GravMap  $m$  contains two voxel maps: (1) a spatial cost map  $m_c$ , with lower values near the sub-goal and higher costs further away, and (2) a gripper openness map  $m_o$ , indicating where the gripper should open or close. As shown in Fig. 2(a), GravMaps are generated differently for training and inference. In training, they are identified from expert demonstrations using the sub-goal keypose discovery method. During inference, pre-trained models generate them from language instructions and observed images.

**GravMap Synthesis with Sub-goal keypose Discovery during Training.** We define each sub-task stage in 3D manipulation as: (1) the process where the robotic end-effector transitions from not touching an object to making contact, or (2) the interaction between the end-effector or tool and a new object, where a series of operations are performed before disengaging. To efficiently segment these sub-task stages and find sub-goals, we build upon the existing keypose discovery method (James & Davison, 2022) and propose a novel data distillation method called **sub-goal keypose discovery**.

The sub-goal keypose discovery process iterates over each keypose  $K_p^i \in \{K_p\}_1^{N_k}$ , where  $N_k$  is the number of keyposes in a task. For each keypose, the corresponding observation-action pair  $(o_{K_p^i}, a_{K_p^i})$  is passed to the function  $S_K$ , which outputs a Boolean value to determine whether the given keypose should be discovered as a sub-goal keypose. The decision is made based on whether the keypose

**Algorithm 1:** GravMap Generation Process

**Input:** End-effector position  $g^{\text{pos}}$ , gripper openness  $g^{\text{open}}$ , map size  $S_m$ , offset range  $\beta_o$ , radius  $\beta_r$ , downsample ratio  $\beta_d$ , number of sampled points  $N_p$

**Output:** GravMap  $m$

**begin**

```

// Initialize spatial cost map  $m_c$  and gripper map  $m_g$  with size  $S_m^3$ 
Initialize  $m_c$  and  $m_g$  with shape  $S_m \times S_m \times S_m$ ;
// Convert  $g^{\text{pos}}$  from world coordinates  $(x, y, z)$  to voxel coordinates  $(i, j, k)$ 
Extract  $(x, y, z) \leftarrow g^{\text{pos}}$ ; Convert  $(x, y, z)$  to voxel coordinates  $(i, j, k)$ ;
// Apply random offsets  $\delta_i, \delta_j, \delta_k$  to  $(i, j, k)$  for data augmentation
Sample  $\delta_i, \delta_j, \delta_k \sim \text{Uniform}(-\beta_o, \beta_o)$ ;
Update voxel coordinates:  $(i', j', k') = (i + \delta_i, j + \delta_j, k + \delta_k)$ ;
// Set  $m_c$  at  $(i', j', k')$  to 0 and 1 elsewhere
Set  $m_c(i', j', k') = 0$ ;
Set  $m_c(u, v, w) = 1$  for all other voxels  $(u, v, w)$ ;
// Compute Euclidean distance from  $(i', j', k')$  for all  $(u, v, w)$ 
For each voxel  $(u, v, w)$ , compute  $D(u, v, w) = \sqrt{(u - i')^2 + (v - j')^2 + (w - k')^2}$ 
Normalize  $m_c(u, v, w) = \frac{D(u, v, w)}{\max D}$ ;
// Set  $m_g$  within radius  $\beta_r$  of  $(i', j', k')$ 
Set  $m_g(u, v, w) = g^{\text{open}}$  for voxels where  $D(u, v, w) \leq \beta_r$ ;
Downsample  $m_c$  and  $m_g$  by  $\beta_d$ ;
Select  $N_p$  points  $\{v_p\}$  from the downsampled  $m_c$  using Farthest Point Sampling (FPS);
// Construct GravMap  $m$  using sampled points
Form  $m = \{(v_p, m_c(v_p), m_g(v_p))\}_{p=1}^{N_p}$ ;
return  $m$ ;

```

satisfies the discovery constraint:  $S_K((o_{K_p^i}, a_{K_p^i})) = \begin{cases} 1, & \text{if discovery constraints are met} \\ 0, & \text{otherwise} \end{cases}$ . The

function  $S_K$  can incorporate multiple constraints. In our paper, we define two constraints for  $S_K$ , depending on the type of manipulation task, as shown in Fig. 3: (1) For grasping tasks, such as “*take the chicken off the grill*”, sub-goal keyposes are discovered based on the following constraints: a change in the gripper’s open/close state and a significant change in touch force. (2) For contact-based tasks, such as “*push the \_\_\_ button*”, sub-goal keyposes are discovered solely based on significant changes in touch force. For more details on sub-goal keypose discovery, please refer to Appendix A.1.

After discovering the sub-goal keyposes, the sub-task stages can be quickly segmented, and the corresponding sub-goals can be identified. The end-effector position  $g^{\text{pos}}$  and gripper openness  $g^{\text{open}}$  at these sub-goals are then input to the *Gravmap generator* to generate the GravMaps  $m$  for training. The process of the GravMap generator is illustrated in Algorithm 1, adapted from Huang et al. (2023).

**GravMap Synthesis with Foundation Model during Inference.** During the inference phase, we use pre-trained foundation models to synthesize GravMaps. First, to enable the robot to tie the task-related words with their manifestation in the 3D environment, we introduce a Set-of-Mark (SoM) (Yang et al., 2023a)-based Detector. This Detector uses Semantic-SAM (Li et al., 2023) to perform semantic segmentation on the observed RGB images and assigns numerical tags to the segmented regions. Next, the Detector uses GPT-4o to select task-relevant objects and their corresponding tags from the labeled images as contextual information  $\mathcal{C}$ . Based on the task instructions  $\ell$  and the context  $\mathcal{C}$  provided by the Detector, we apply the LLM-based Planner proposed by Huang et al. to infer a series of text-based sub-goals. Then, an LLM-based Composer (Huang et al., 2023) recursively generates code to parse each sub-goal. During execution, the code uses the context  $\mathcal{C}$  to obtain the end-effector positions  $g^{\text{pos}}$  and gripper openness states  $g^{\text{open}}$  corresponding to each sub-goal. Finally,  $g^{\text{pos}}$  and  $g^{\text{open}}$  are fed into the *GravMap generator* shown in Algorithm 1, to generate the GravMaps. Details of this process can be found in Appendix A.2.2.

We synthesize the GravMaps via sub-goal keypose discovery during training or foundation models during inference. GravMaps are then  $m$  downsampled using farthest point sampling (FPS) and encoded into token  $t_m$  with the DP3 (Ze et al., 2024) encoder, a lightweight MLP network.

### 3.3 GRAVMAPS GUIDED ACTION DIFFUSION

After obtaining the GravMaps, they can be used to guide the action diffusion process, as shown in Fig. 2(b). Before the diffusion process begins, the robot should first perceive the 3D environment.

**3D Scene Perception.** Building on previous works (Gervet et al., 2023; Ke et al., 2024), we use a 3D scene encoder to transform language instructions and multi-view RGB-D images into scene tokens, enhancing the robot’s 3D scene perception. RGB images are encoded using a pre-trained CLIP ResNet50 backbone (Radford et al., 2021) and a feature pyramid network. These features are lifted into 3D feature clouds using 3D positions derived from depth images and camera intrinsics. Simultaneously, the CLIP language encoder converts task instructions into language tokens. These tokens interact with the 3D feature cloud to generate scene tokens ( $t_s$ ), enabling the robot to capture 3D environmental information.

**GravMaps Guided Action Diffusion.** GravMAD builds upon the 3D trajectory diffusion architecture introduced by 3D Diffuser Actor (Ke et al., 2024) and further integrates GravMap tokens  $t_m$  to guide the action diffusion process. Specifically, GravMAD models policy learning as the reconstruction of the robot’s end-effector pose using diffusion probabilistic models (DDPMs) (Ho et al., 2020). The end-effector pose is represented as  $e = (a^{\text{pos}}, a^{\text{rot}})$ . Starting with Gaussian noise  $e_K = (a_K^{\text{pos}}, a_K^{\text{rot}})$ , the denoising networks  $\epsilon_\theta^{\text{pos}}$  and  $\epsilon_\theta^{\text{rot}}$  perform  $K$  iterative steps to progressively reconstruct the clean pose  $e_0 = (a_0^{\text{pos}}, a_0^{\text{rot}})$ :

$$\begin{aligned} a_{k-1}^{\text{pos}} &= \alpha \left( a_k^{\text{pos}} - \gamma \epsilon_\theta^{\text{pos}}(e_k, k, p, t_s, t_m) + \mathcal{N}(0, \sigma^2 I) \right), \\ a_{k-1}^{\text{rot}} &= \alpha \left( a_k^{\text{rot}} - \gamma \epsilon_\theta^{\text{rot}}(e_k, k, p, t_s) + \mathcal{N}(0, \sigma^2 I) \right), \end{aligned} \quad (1)$$

where  $\alpha$ ,  $\gamma$ , and  $\sigma$  are functions of the iteration step  $k$ , determined by the noise schedule.  $\mathcal{N}(0, \sigma^2 I)$  is Gaussian noise. Here,  $p$  represents proprioceptive information (a short action history). The denoising networks use 3D relative position attention layers (Gervet et al., 2023; Xian et al., 2023; Ke et al., 2024), with FiLM (Perez et al., 2018) conditioning applied to each layer based on proprioception  $p$  and denoising step  $k$ . As shown in Fig. 2(b), after passing through linear layers,  $a_k^{\text{pos}}$  and  $a_k^{\text{rot}}$  are concatenated and attend to the 3D scene tokens  $t_s$  via cross-attention. A self-attention layer then refines this representation to produce end-effector contextual features. These features are processed by five prediction heads: the *Position Head*, *Rotation Head*, *Openness Head*, *Auxiliary Openness Head*, and *Auxiliary Position Head*.

The first two prediction heads predict the noise added to the original pose using the  $L1$  norm, with the losses defined as:

$$\begin{aligned} \mathcal{L}_{\text{pos}} &= \|\epsilon_k^{\text{pos}} - \epsilon_\theta^{\text{pos}}(e_k, k, p, t_s, t_m)\|, \\ \mathcal{L}_{\text{rot}} &= \|\epsilon_k^{\text{rot}} - \epsilon_\theta^{\text{rot}}(e_k, k, p, t_s)\|, \end{aligned} \quad (2)$$

where iteration  $k$  is randomly selected, and  $\epsilon_k^{\text{pos}}$  and  $\epsilon_k^{\text{rot}}$  are randomly sampled as the ground truth noise.

The third prediction head is used to predict the gripper’s open/close state, and we use binary cross-entropy (BCE) loss for supervision:

$$\mathcal{L}_{\text{open}} = \text{BCE} \left( f_\theta^{\text{open}}(e_k, k, p, t_s, t_m), a^{\text{open}} \right) \quad (3)$$

The last two prediction heads enable GravMAD to better focus on the ideal end-effector pose at sub-goals, with the loss functions defined as follows:

$$\begin{aligned} \mathcal{L}_{\text{aux\_pos}} &= \|g^{\text{pos}} - f_\theta^{\text{aux\_pos}}(e_k, k, p, t_s, t_m)\|, \\ \mathcal{L}_{\text{aux\_open}} &= \text{BCE} \left( f_\theta^{\text{aux\_open}}(e_k, k, p, t_s, t_m), g^{\text{open}} \right), \end{aligned} \quad (4)$$

where  $f_\theta$  represents the pose prediction network in GravMAD, while  $g^{\text{pos}}$  and  $g^{\text{open}}$  denote the ground truth sub-goal positions and gripper openness, respectively.

In addition to the losses related to robot actions mentioned above, a contrastive learning loss is applied to enhance feature representations from GravMaps. Positive pairs are features from the same GravMap, while negative pairs come from different GravMaps. In each forward pass, one GravMap

is extracted from the dataset, and  $N - 1$  different GravMaps are randomly generated. The loss maximizes similarity between positive pairs and minimizes it between negative pairs:

$$\mathcal{L}_{\text{con}} = -\frac{1}{N} \sum_{i=1}^N \log \frac{\exp(f_{g_i} \cdot f_{g_i}^+ / T)}{\sum_{j=1}^N \exp(f_{g_i} \cdot f_{g_j} / T)}, \quad (5)$$

where  $T$  is the temperature parameter,  $f_{g_i}$  represents the feature of the  $i$ -th sample, and  $f_{g_i}^+$  represents the positive feature of the  $i$ -th sample.

At this stage, the training objective of GravMAD can be formulated by combining the losses from Eq.2, 3, 4, and 5 as follows:

$$\mathcal{L}_{\text{GravMAD}} = \mathcal{L}_{\text{open}} + \omega_1 \cdot \mathcal{L}_{\text{pos}} + \omega_2 \cdot \mathcal{L}_{\text{rot}} + \omega_3 \cdot \mathcal{L}_{\text{aux\_pos}} + \mathcal{L}_{\text{aux\_open}} + \omega_4 \cdot \mathcal{L}_{\text{con}}, \quad (6)$$

where  $\omega_1, \omega_2, \omega_3, \omega_4$  are adjustable hyperparameters. For more detailed implementation of GravMap and GravMAD, please refer to Appendix A.

## 4 EXPERIMENTS

We aim to answer the following questions: **(i)** Can GravMAD achieve superior generalization in novel 3D manipulation tasks compared to SOTA models? (See Sec. 4.2) **(ii)** Is GravMAD’s performance competitive on the 3D manipulation tasks encountered during training? (See Sec. 4.3) **(iii)** What key design elements contribute significantly to GravMAD’s overall performance? (See Sec. 4.4)

### 4.1 ENVIRONMENTAL SETUP

To thoroughly investigate these questions, we conduct our experiments on a representative instruction-following 3D manipulation benchmark, RL Bench (James et al., 2020b). We design two types of tasks to provide a comprehensive evaluation of GravMAD. **1) Base tasks.** To evaluate GravMAD’s performance across 3D manipulation tasks encountered during training, we select 12 base tasks from RL Bench’s 100 language-conditioned tasks, each featuring 2 to 60 variations in instructions, such as handling objects of different colors or quantities. For each base task, we collect 20 demonstrations for training and evaluate the final checkpoints using 3 random seeds over 25 episodes. Detailed descriptions of these tasks are provided in Appendix B.1. **2) Novel tasks.** To further test GravMAD’s generalization capabilities, we modify the scene configurations or task instructions of several base tasks to create 8 novel tasks. These modifications introduce significant challenges for the robot regarding instruction comprehension, environmental perception, and policy generalization, as described in Appendix B.2. For each novel task, we evaluate the final checkpoints trained on the 12 base tasks. We use 3 random seeds over 25 episodes for each novel task. For all tasks, we use a front-view  $256 \times 256$  RGB-D camera and a Franka Panda robot with parallel grippers.

**Baselines.** We compare GravMAD against various baselines, covering both foundation model-based and imitation learning-based methods. For the foundation model-based approach, we use **VoxPoser** (Huang et al., 2023) as the baseline. VoxPoser leverages GPT-4 to generate code for constructing value maps, which are then used by a heuristic-based motion planner to synthesize robotic arm trajectories. We reproduce this baseline in our tasks using prompt templates from Huang et al. and our SoM-based Detector, with five camera viewpoints in RL Bench. For the imitation learning-based baselines, we select: (1) **3D Diffuser Actor** (Ke et al., 2024), which combines 3D scene representations with a diffusion policy for robotic manipulation tasks. To highlight instruction-following tasks, we use the enhanced language-conditioned version provided by Ke et al.; and (2) **Act3D** (Gervet et al., 2023), which uses a 3D feature field within a policy transformer to represent the robot’s workspace. Differences between GravMAD and these baselines are detailed in Appendix A.4.

**Training and Evaluation Details.** GravMAD runs in a multi-task setting during both the training and testing phases. All models complete 600k training iterations on an NVIDIA RTX4090 GPU, with the final checkpoint selected using three random seeds for evaluation. During testing, except for the novel task “*Push Buttons Light*”, which must be completed within 3 time steps, all other tasks must be finished within 25 time steps; otherwise, they are considered failures. Evaluation metrics include average success rate and rank. The success rate measures the proportion of tasks completed based on language instructions. Meanwhile, the average rank calculates the average of each model’s rankings

Models	Avg. Success $\uparrow$	Avg. Rank $\downarrow$	Close Drawer	Close Jar Banana	Close Jar Distractor	Condition Block	Meat On Grill	Open Drawer Small	Stack cups blocks	Push Buttons Light
Voxposer (Huang et al., 2023)	34.29	2.6	96.00 $\pm$ 4.00	17.33 $\pm$ 19.73	22.67 $\pm$ 10.07	25.00 $\pm$ 23.26	38.67 $\pm$ 12.22	6.67 $\pm$ 2.31	0.00 $\pm$ 0.00	68.00 $\pm$ 18.33
Act3D (Gervet et al., 2023)	17.83	3.5	66.67 $\pm$ 9.24	29.33 $\pm$ 9.24	41.33 $\pm$ 4.62	0.00 $\pm$ 0.00	1.33 $\pm$ 2.31	2.67 $\pm$ 4.62	0.00 $\pm$ 0.00	1.33 $\pm$ 2.31
3D Diffuser Actor (Ke et al., 2024)	29.38	2.9	81.33 $\pm$ 6.11	48.00 $\pm$ 4.00	42.67 $\pm$ 4.62	27.00 $\pm$ 10.15	0.00 $\pm$ 0.00	2.67 $\pm$ 4.62	2.67 $\pm$ 2.31	30.67 $\pm$ 12.86
GravMAD (VLM)	<b>62.92</b>	1.0	<b>97.33</b> $\pm$ 2.31	<b>84.00</b> $\pm$ 0.00	<b>86.67</b> $\pm$ 2.31	<b>74.00</b> $\pm$ 11.14	<b>45.33</b> $\pm$ 4.62	<b>21.33</b> $\pm$ 12.86	<b>18.67</b> $\pm$ 2.31	<b>76.00</b> $\pm$ 8.00
Performance gain	<b>+28.63</b>	-	<b>+1.33</b>	<b>+36.00</b>	<b>+44.00</b>	<b>+47.00</b>	<b>+6.66</b>	<b>+14.66</b>	<b>+16.00</b>	<b>+8.00</b>

Table 1: **Generalization to 8 novel RLbench tasks.** Evaluations on 8 novel tasks are conducted using 3 seeds, with 25 test episodes per task, utilizing the final checkpoints from training on 12 base tasks. Performance gains are compared to the best-performing baselines, indicated by underlines.

Models	Avg. Success $\uparrow$	Avg. Rank $\downarrow$	Close Jar	Open Drawer	Meat off Grill	Slide Block	Put in Drawer
Voxposer (Huang et al., 2023)	15.11	4.5	12.00 $\pm$ 10.58	10.67 $\pm$ 8.33	45.33 $\pm$ 24.44	0.00 $\pm$ 0.00	0.00 $\pm$ 0.00
Act3D (Gervet et al., 2023)	34.11	4.3	61.33 $\pm$ 4.62	41.33 $\pm$ 4.62	60.0 $\pm$ 6.92	78.67 $\pm$ 2.31	49.33 $\pm$ 10.07
3D Diffuser Actor (Ke et al., 2024)	<u>55.81</u>	2.3	<u>66.67</u> $\pm$ 2.31	<u>88.00</u> $\pm$ 6.93	<u>88.00</u> $\pm$ 4.00	<u>84.00</u> $\pm$ 0.00	<u>94.67</u> $\pm$ 2.31
GravMAD (Manual)	<b>69.17</b>	1.3	<b>100.00</b> $\pm$ 0.00	76.67 $\pm$ 4.62	<b>89.33</b> $\pm$ 2.31	<b>93.33</b> $\pm$ 2.31	78.67 $\pm$ 6.11
Performance gain	<b>+13.36</b>	-	<b>+33.33</b>	-13.33	<b>+1.33</b>	<b>+9.33</b>	-16.00
GravMAD (VLM)	<b>56.72</b>	2.1	<b>100.00</b> $\pm$ 0.00	58.67 $\pm$ 2.31	70.67 $\pm$ 2.31	80.00 $\pm$ 0.00	61.33 $\pm$ 9.24
Performance gain	<b>+0.91</b>	-	<b>+33.33</b>	-29.33	-17.33	-4.00	-33.34

Models	Push Buttons	Stack Blocks	Place Cups	Place Wine	Screw Bulb	Insert Peg	Stack Cups
Voxposer (Huang et al., 2023)	80.00 $\pm$ 13.86	16.00 $\pm$ 12.00	6.67 $\pm$ 8.33	5.33 $\pm$ 2.31	4.00 $\pm$ 4.00	0.00 $\pm$ 0.00	1.33 $\pm$ 2.31
Act3D (Gervet et al., 2023)	66.67 $\pm$ 2.31	0.00 $\pm$ 0.00	0.00 $\pm$ 0.00	45.33 $\pm$ 2.31	6.67 $\pm$ 2.31	0.00 $\pm$ 0.00	0.00 $\pm$ 0.00
3D Diffuser Actor (Ke et al., 2024)	<u>94.67</u> $\pm$ 2.31	13.67 $\pm$ 2.89	5.33 $\pm$ 6.11	<u>82.67</u> $\pm$ 2.31	<u>29.33</u> $\pm$ 2.31	<u>2.67</u> $\pm$ 4.62	<u>20.00</u> $\pm$ 0.00
GravMAD (Manual)	<b>98.67</b> $\pm$ 2.31	<b>56.67</b> $\pm$ 4.62	5.33 $\pm$ 2.31	77.33 $\pm$ 4.62	<b>66.67</b> $\pm$ 6.11	<b>32.00</b> $\pm$ 6.93	<b>57.33</b> $\pm$ 2.31
Performance gain	<b>+4.00</b>	<b>+40.67</b>	-1.34	-5.34	<b>+37.34</b>	<b>+29.33</b>	<b>+37.33</b>
GravMAD (VLM)	<b>97.33</b> $\pm$ 2.31	<b>51.33</b> $\pm$ 6.11	5.33 $\pm$ 4.62	33.33 $\pm$ 4.62	<b>54.67</b> $\pm$ 6.11	<b>18.67</b> $\pm$ 4.62	<b>49.33</b> $\pm$ 2.31
Performance gain	<b>+2.66</b>	<b>+35.33</b>	-1.34	-49.34	<b>+25.34</b>	<b>+16.00</b>	<b>+29.33</b>

Table 2: **Multi-task test results on 12 base tasks.** All models are trained on 12 base tasks with 20 demonstrations each. Final checkpoints are evaluated across 3 seeds with 25 test episodes per task. Performance gains are compared to the best-performing baselines.

across all tasks, reflecting the model’s overall performance in the tasks. Two settings are used for generating context  $\mathcal{C}$  during testing: *Manual* and *VLM*. In the manual setting, we manually provide the Detector with the precise 3D coordinates of task-related objects in the simulation to generate accurate context. In the VLM setting, we use a Detector implemented with SoM and GPT-4o to locate task-related objects and generate context.

#### 4.2 GENERALIZATION PERFORMANCE OF GRAVMAD TO NOVEL TASKS

In Table 1, we present the generalization performance of models trained on 12 base tasks when tested on 8 novel tasks, along with visualized trajectories from two of these tasks. The results show that changes in task scenarios and instructions negatively impact the test performance of all pre-trained models to some extent. However, GravMAD exhibits superior generalization across all 8 novel tasks compared to the baseline models. In terms of average success rate, GravMAD outperforms VoxPoser, Act3D, and 3D Diffuser Actor by **28.63%**, **45.09%**, and **33.54%**, respectively. VoxPoser leverages large models to achieve a certain level of performance on novel tasks, but its heuristic motion planner fails to grasp object properties and task interaction conditions, leading to poor results on tasks requiring fine manipulation, as shown in the trajectory visualizations. Similarly, 3D Diffuser Actor and Act3D struggle to transfer skills from training to novel tasks, primarily due to overfitting to training-specific tasks, which hampers generalization. In contrast, GravMAD uses VLM-generated GravMaps to guide action diffusion, enabling effective object interaction and strong performance on novel tasks. These results clearly demonstrate GravMAD’s superior generalization, surpassing all baseline models.

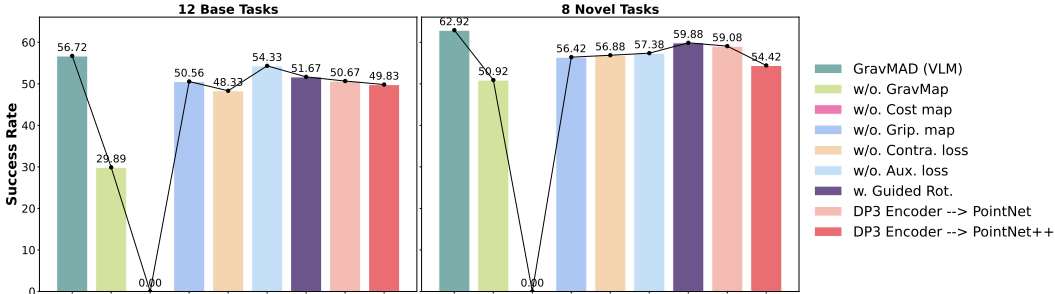


Figure 4: **Ablation Studies.** We evaluate the impact of key design elements by reporting the average success rates across 12 base tasks and 8 novel tasks. In the results, “→” denotes replacement, “w/o” indicates “without”, and “w.” signifies “with”.

### 4.3 TEST PERFORMANCE OF GRAVMAD ON BASE TASKS

Table 2 compares the performance of all models on 12 base tasks. GravMAD (Manual) outperforms Act3D and Voxposer across all tasks and exceeds the best baseline, 3D Diffuser Actor, in 9 out of 12 tasks, with an average success rate improvement of **13.36%**. Despite the Detector’s coarse SoM positioning affecting GravMAD (VLM)’s performance, it still outperforms Act3D and Voxposer on all tasks, with a **0.91%** higher average success rate than 3D Diffuser Actor. These results clearly show that GravMAD remains highly competitive even on previously seen tasks. As long as task-related object positions are accurate, the generated GravMap effectively reflects sub-goals and guides action diffusion, enabling precise execution by GravMAD. GravMAD (Manual) underperforms 3D Diffuser Actor in the “*Open Drawer*”, “*Put in Drawer*”, and “*Place Wine*” tasks due to slight deviations between the manually provided object positions and the sub-goals. In high-precision tasks, even small deviations can impact performance. For example, in the “*Open Drawer*” task, the robot needs to grasp the center of the small handle for optimal performance. After manually adjusting the sub-goal to better align with the handle, performance improved. GravMAD (VLM) also struggles in tasks like “*Place Wine*” due to inaccuracies in the object positions provided by the Detector, especially when Semantic SAM fails to provide precise locations or the camera doesn’t capture the full scene. For further analysis of failure cases, please refer to Appendix B.3.

### 4.4 ABLATIONS

Extensive ablation studies are conducted to analyze the role of each key design element in GravMAD, with the results shown in Fig 4. The following findings are revealed: **1) Impact of replacing GravMaps with specific sub-goal position and openness:** Training policies only with sub-goals  $g^{\text{pos}}$  and  $g^{\text{open}}$  (w/o. GravMap) leads to a significant drop in task success rates. These policies tend to focus on specific points rather than broader regions, making them more prone to inaccuracies from slight positional changes. **2) Importance of both cost map and gripper map in GravMaps:** The combination of the cost map and gripper map within GravMaps is essential for guiding the model’s attention to sub-goal locations and ensuring effective gripper usage. The absence of the gripper map causes a moderate decline in performance (w/o. Grip. map). In contrast, omitting the cost map leads to complete task failure, as the model predicts actions with non-unit quaternions, highlighting the cost map’s critical importance (w/o. Cost map). **3) Significance of contrastive learning loss and auxiliary losses:** Removing the contrastive learning loss  $\mathcal{L}_{\text{con}}$  results in highly similar features from the point cloud encoder, diminishing their effectiveness in action denoising and leading to a decline in model performance (w/o. Contra. loss). Similarly, the absence of auxiliary losses  $\mathcal{L}_{\text{aux\_pos}}$  and  $\mathcal{L}_{\text{aux\_open}}$  weakens the model’s focus on sub-goals, leading to a noticeable drop in performance (w/o Aux. loss). **4) Effect of GravMap tokens on guiding rotation actions:** Conditioning rotation actions with GravMap tokens in the action diffusion process results in a performance drop, likely due to the inherent nature of rotation actions, which makes them difficult to be guided explicitly through value maps (w. Guided Rot.). **5) Impact of different point cloud encoders on GravMap performance.** Replacing the DP3 encoder in GravMAD with PointNet (Qi et al., 2017a) (DP3 Encoder → PointNet) or PointNet++ (Qi et al., 2017b) (DP3 Encoder → PointNet++) leads to a performance decline. We suspect that lightweight encoders help prevent overfitting to training data details, enhancing GravMAD’s generalization ability across different tasks or unseen data.

## 5 CONCLUSION AND DISCUSSION

In this paper, we introduce GravMAD, a novel action diffusion framework that facilitates generalized 3D manipulation using sub-goals. GravMAD grounds language instructions into spatial subgoals within the 3D workspace through grounded spatial value maps (GravMaps). During training, these GravMaps are generated from demonstrations by Sub-goal Keyposes Discovery. In the inference phase, GravMaps are constructed by leveraging foundational models to directly predict sub-goals. Consequently, GravMAD seamlessly integrates the precision of imitation learning with the strong generalization capabilities of foundational models, leading to superior performance across a variety of manipulation tasks. Extensive experiments on the RL Bench benchmark show that GravMAD achieves competitive performance on training tasks. It also generalizes well to novel tasks, demonstrating its potential for practical use across diverse 3D environments. Despite its promising results, GravMAD has some limitations. First, its effectiveness relies heavily on prompt engineering, which can be challenging for inexperienced users. Additionally, the visual-language models (VLMs) have limited detection capabilities and are sensitive to changes in camera perspective, affecting performance and preventing optimal efficiency and accuracy. Future work will address these issues to enhance the model’s performance, expand its applicability, and validate its use on real-world robots.

## REFERENCES

- Brenna D. Argall, Sonia Chernova, Manuela M. Veloso, and Brett Browning. A survey of robot learning from demonstration. *Robotics Auton. Syst.*, 57(5):469–483, 2009.
- Anthony Brohan, Noah Brown, Justice Carbajal, Yevgen Chebotar, Joseph Dabis, Chelsea Finn, Keerthana Gopalakrishnan, Karol Hausman, Alexander Herzog, Jasmine Hsu, Julian Ibarz, Brian Ichter, Alex Irpan, Tomas Jackson, Sally Jesmonth, Nikhil J. Joshi, Ryan Julian, Dmitry Kalashnikov, Yuheng Kuang, Isabel Leal, Kuang-Huei Lee, Sergey Levine, Yao Lu, Utsav Malla, Deeksha Manjunath, Igor Mordatch, Ofir Nachum, Carolina Parada, Jodilyn Peralta, Emily Perez, Karl Pertsch, Jornell Quiambao, Kanishka Rao, Michael S. Ryoo, Grecia Salazar, Pannag R. Sanketi, Kevin Sayed, Jaspiar Singh, Sumedh Sontakke, Austin Stone, Clayton Tan, Huong T. Tran, Vincent Vanhoucke, Steve Vega, Quan Vuong, Fei Xia, Ted Xiao, Peng Xu, Sichun Xu, Tianhe Yu, and Brianna Zitkovich. RT-1: robotics transformer for real-world control at scale. In *Proceedings of Robotics: Science and Systems (RSS)*, 2023a.
- Anthony Brohan, Yevgen Chebotar, Chelsea Finn, Karol Hausman, Alexander Herzog, Daniel Ho, Julian Ibarz, Alex Irpan, Eric Jang, Ryan Julian, et al. Do as i can, not as i say: Grounding language in robotic affordances. In *Conference on robot learning (CoRL)*, pp. 287–318. PMLR, 2023b.
- Shizhe Chen, Ricardo Garcia Pinel, Cordelia Schmid, and Ivan Laptev. Polarnet: 3d point clouds for language-guided robotic manipulation. In *Conference on Robot Learning (CoRL)*, pp. 1761–1781. PMLR, 2023.
- Danny Driess, Fei Xia, Mehdi S. M. Sajjadi, Corey Lynch, Aakanksha Chowdhery, Brian Ichter, Ayzan Wahid, Jonathan Tompson, Quan Vuong, Tianhe Yu, Wenlong Huang, Yevgen Chebotar, Pierre Sermanet, Daniel Duckworth, Sergey Levine, Vincent Vanhoucke, Karol Hausman, Marc Toussaint, Klaus Greff, Andy Zeng, Igor Mordatch, and Pete Florence. Palm-e: An embodied multimodal language model. In Andreas Krause, Emma Brunskill, Kyunghyun Cho, Barbara Engelhardt, Sivan Sabato, and Jonathan Scarlett (eds.), *International Conference on Machine Learning (ICML)*, volume 202, pp. 8469–8488. PMLR, 2023.
- Theophile Gervet, Zhou Xian, Nikolaos Gkanatsios, and Katerina Fragkiadaki. Act3d: 3d feature field transformers for multi-task robotic manipulation. In *Conference on Robot Learning (CoRL)*, pp. 3949–3965. PMLR, 2023.
- Ankit Goyal, Jie Xu, Yijie Guo, Valts Blukis, Yu-Wei Chao, and Dieter Fox. Rvt: Robotic view transformer for 3d object manipulation. In *Conference on Robot Learning (CoRL)*, pp. 694–710. PMLR, 2023.
- Ankit Goyal, Valts Blukis, Jie Xu, Yijie Guo, Yu-Wei Chao, and Dieter Fox. Rvt2: Learning precise manipulation from few demonstrations. *Proceedings of Robotics: Science and Systems (RSS)*, 2024.

- Jonathan Ho, Ajay Jain, and Pieter Abbeel. Denoising diffusion probabilistic models. *Advances in neural information processing systems (NeurIPS)*, 33:6840–6851, 2020.
- Yafei Hu, Quanting Xie, Vidhi Jain, Jonathan Francis, Jay Patrikar, Nikhil Keetha, Seungchan Kim, Yaqi Xie, Tianyi Zhang, Zhibo Zhao, et al. Toward general-purpose robots via foundation models: A survey and meta-analysis. *arXiv preprint arXiv:2312.08782*, 2023a.
- Yingdong Hu, Fanqi Lin, Tong Zhang, Li Yi, and Yang Gao. Look before you leap: Unveiling the power of gpt-4v in robotic vision-language planning. *arXiv preprint arXiv:2311.17842*, 2023b.
- Haoxu Huang, Fanqi Lin, Yingdong Hu, Shengjie Wang, and Yang Gao. Copa: General robotic manipulation through spatial constraints of parts with foundation models. *arXiv preprint arXiv:2403.08248*, 2024.
- Wenlong Huang, Pieter Abbeel, Deepak Pathak, and Igor Mordatch. Language models as zero-shot planners: Extracting actionable knowledge for embodied agents. In *International Conference on Machine Learning (ICML)*, pp. 9118–9147. PMLR, 2022.
- Wenlong Huang, Chen Wang, Ruohan Zhang, Yunzhu Li, Jiajun Wu, and Li Fei-Fei. Voxposer: Composable 3d value maps for robotic manipulation with language models. In *Conference on Robot Learning (CoRL)*, pp. 540–562. PMLR, 2023.
- Stephen James and Andrew J Davison. Q-attention: Enabling efficient learning for vision-based robotic manipulation. *IEEE Robotics and Automation Letters*, 7(2):1612–1619, 2022.
- Stephen James, Zicong Ma, David Rovick Arrojo, and Andrew J. Davison. Rlbench: The robot learning benchmark & learning environment. *IEEE Robotics and Automation Letter*, 5(2):3019–3026, 2020a.
- Stephen James, Zicong Ma, David Rovick Arrojo, and Andrew J Davison. Rlbench: The robot learning benchmark & learning environment. *IEEE Robotics and Automation Letters*, 5(2):3019–3026, 2020b.
- Stephen James, Kentaro Wada, Tristan Laidlow, and Andrew J Davison. Coarse-to-fine q-attention: Efficient learning for visual robotic manipulation via discretisation. In *Proceedings of the IEEE/CVF Conference on Computer Vision and Pattern Recognition (CVPR)*, pp. 13739–13748, 2022.
- Eric Jang, Alex Irpan, Mohi Khansari, Daniel Kappler, Frederik Ebert, Corey Lynch, Sergey Levine, and Chelsea Finn. Bc-z: Zero-shot task generalization with robotic imitation learning. In *Conference on Robot Learning (CoRL)*, pp. 991–1002. PMLR, 2022.
- Tsung-Wei Ke, Nikolaos Gkanatsios, and Katerina Fragkiadaki. 3d diffuser actor: Policy diffusion with 3d scene representations. In *Conference on Robot Learning (CoRL)*. PMLR, 2024.
- Sebastian Klemm, Jan Oberländer, Andreas Hermann, Arne Roennau, Thomas Schamm, J Marius Zollner, and Rüdiger Dillmann. Rrt\*-connect: Faster, asymptotically optimal motion planning. In *2015 IEEE international conference on robotics and biomimetics (ROBIO)*, pp. 1670–1677. IEEE, 2015.
- Feng Li, Hao Zhang, Peize Sun, Xueyan Zou, Shilong Liu, Jianwei Yang, Chunyuan Li, Lei Zhang, and Jianfeng Gao. Semantic-sam: Segment and recognize anything at any granularity. *arXiv preprint arXiv:2307.04767*, 2023.
- Xinghang Li, Minghuan Liu, Hanbo Zhang, Cunjun Yu, Jie Xu, Hongtao Wu, Chilam Cheang, Ya Jing, Weinan Zhang, Huaping Liu, Hang Li, and Tao Kong. Vision-language foundation models as effective robot imitators. In *International Conference on Learning Representations (ICLR)*, 2024.
- Jacky Liang, Wenlong Huang, Fei Xia, Peng Xu, Karol Hausman, Brian Ichter, Pete Florence, and Andy Zeng. Code as policies: Language model programs for embodied control. In *2023 IEEE International Conference on Robotics and Automation (ICRA)*, pp. 9493–9500. IEEE, 2023.
- OpenAI. GPT-4 technical report. *CoRR*, abs/2303.08774, 2023.

- Abhishek Padalkar, Ajinkya Jain, Alex Bewley, Alexander Herzog, Alex Irpan, Alexander Khazatsky, Anant Raj, Anikait Singh, Anthony Brohan, Antonin Raffin, Ayzaan Wahid, Ben Burgess-Limerick, Beomjoon Kim, Bernhard Schölkopf, Brian Ichter, Cewu Lu, Charles Xu, Chelsea Finn, Chenfeng Xu, Cheng Chi, Chenguang Huang, Christine Chan, Chuer Pan, Chuyuan Fu, Coline Devin, Danny Driess, Deepak Pathak, Dhruv Shah, Dieter Büchler, Dmitry Kalashnikov, Dorsa Sadigh, Edward Johns, Federico Ceola, Fei Xia, Freek Stulp, Gaoyue Zhou, Gaurav S. Sukhatme, Gautam Salhotra, Ge Yan, Giulio Schiavi, Gregory Kahn, Hao Su, Haoshu Fang, Haochen Shi, Heni Ben Amor, Henrik I. Christensen, Hiroki Furuta, Homer Walke, Hongjie Fang, Igor Mordatch, Ilija Radosavovic, and et al. Open x-embodiment: Robotic learning datasets and RT-X models. In *IEEE International Conference on Robotics and Automation (ICRA)*, pp. 6892–6903. IEEE, 2024.
- Ethan Perez, Florian Strub, Harm De Vries, Vincent Dumoulin, and Aaron Courville. Film: Visual reasoning with a general conditioning layer. In *Proceedings of the AAAI conference on artificial intelligence (AAAI)*, 2018.
- Charles R Qi, Hao Su, Kaichun Mo, and Leonidas J Guibas. Pointnet: Deep learning on point sets for 3d classification and segmentation. In *Proceedings of the IEEE/CVF Conference on Computer Vision and Pattern Recognition (CVPR)*, pp. 652–660, 2017a.
- Charles Ruizhongtai Qi, Li Yi, Hao Su, and Leonidas J Guibas. Pointnet++: Deep hierarchical feature learning on point sets in a metric space. *Advances in neural information processing systems (NeurIPS)*, 30, 2017b.
- Alec Radford, Jong Wook Kim, Chris Hallacy, Aditya Ramesh, Gabriel Goh, Sandhini Agarwal, Girish Sastry, Amanda Askell, Pamela Mishkin, Jack Clark, et al. Learning transferable visual models from natural language supervision. In *International Conference on Machine Learning (ICML)*, pp. 8748–8763. PMLR, 2021.
- SP Sharan, Ruihan Zhao, Zhangyang Wang, Sandeep P Chinchali, et al. Plan diffuser: Grounding llm planners with diffusion models for robotic manipulation. In *Bridging the Gap between Cognitive Science and Robot Learning in the Real World: Progresses and New Directions*, 2024.
- Mohit Shridhar, Lucas Manuelli, and Dieter Fox. Perceiver-actor: A multi-task transformer for robotic manipulation. In *Conference on Robot Learning (CoRL)*, pp. 785–799. PMLR, 2023.
- Homer Rich Walke, Kevin Black, Tony Z. Zhao, Quan Vuong, Chongyi Zheng, Philippe Hansen-Estruch, Andre Wang He, Vivek Myers, Moo Jin Kim, Max Du, Abraham Lee, Kuan Fang, Chelsea Finn, and Sergey Levine. Bridgedata V2: A dataset for robot learning at scale. In Jie Tan, Marc Toussaint, and Kourosh Darvish (eds.), *Conference on Robot Learning (CoRL)*, volume 229, pp. 1723–1736. PMLR, 2023.
- Zhou Xian, Nikolaos Gkanatsios, Theophile Gervet, Tsung-Wei Ke, and Katerina Fragkiadaki. Chaineddiffuser: Unifying trajectory diffusion and keypose prediction for robotic manipulation. In *Conference on Robot Learning (CoRL)*, pp. 2323–2339. PMLR, 2023.
- Annie Xie, Lisa Lee, Ted Xiao, and Chelsea Finn. Decomposing the generalization gap in imitation learning for visual robotic manipulation. In *2024 IEEE International Conference on Robotics and Automation (ICRA)*, pp. 3153–3160. IEEE, 2024.
- Ge Yan, Yueh-Hua Wu, and Xiaolong Wang. Dnact: Diffusion guided multi-task 3d policy learning. *arXiv preprint arXiv:2403.04115*, 2024.
- Jianwei Yang, Hao Zhang, Feng Li, Xueyan Zou, Chunyuan Li, and Jianfeng Gao. Set-of-mark prompting unleashes extraordinary visual grounding in GPT-4V. *CoRR*, abs/2310.11441, 2023a.
- Zhengyuan Yang, Linjie Li, Kevin Lin, Jianfeng Wang, Chung-Ching Lin, Zicheng Liu, and Lijuan Wang. The dawn of llms: Preliminary explorations with gpt-4v(ision). *CoRR*, abs/2309.17421, 2023b.
- Wentao Yuan, Adithyavairavan Murali, Arsalan Mousavian, and Dieter Fox. M2t2: Multi-task masked transformer for object-centric pick and place. In *Conference on Robot Learning (CoRL)*, pp. 3619–3630. PMLR, 2023.

- Yanjie Ze, Ge Yan, Yueh-Hua Wu, Annabella Macaluso, Yuying Ge, Jianglong Ye, Nicklas Hansen, Li Erran Li, and Xiaolong Wang. Gnfactor: Multi-task real robot learning with generalizable neural feature fields. In Jie Tan, Marc Toussaint, and Kourosh Darvish (eds.), *Conference on Robot Learning (CoRL)*, volume 229, pp. 284–301. PMLR, 2023.
- Yanjie Ze, Gu Zhang, Kangning Zhang, Chenyuan Hu, Muhan Wang, and Huazhe Xu. 3d diffusion policy: Generalizable visuomotor policy learning via simple 3d representations. In *Proceedings of Robotics: Science and Systems (RSS)*, 2024.
- Junjie Zhang, Chenjia Bai, Haoran He, Zhigang Wang, Bin Zhao, Xiu Li, and Xuelong Li. Sam-e: Leveraging visual foundation model with sequence imitation for embodied manipulation. In *International Conference on Machine Learning (ICML)*, 2024.
- Tong Zhang, Yingdong Hu, Hanchen Cui, Hang Zhao, and Yang Gao. A universal semantic-geometric representation for robotic manipulation. In *Conference on Robot Learning (CoRL)*, pp. 3342–3363. PMLR, 2023.
- Hongkuan Zhou, Xiangtong Yao, Yuan Meng, Siming Sun, Zhenshan Bing, Kai Huang, and Alois Knoll. Language-conditioned learning for robotic manipulation: A survey. *arXiv preprint arXiv:2312.10807*, 2023.
- Brianna Zitkovich, Tianhe Yu, Sichun Xu, Peng Xu, Ted Xiao, Fei Xia, Jialin Wu, Paul Wohlhart, Stefan Welker, Ayzaan Wahid, Quan Vuong, Vincent Vanhoucke, Huong T. Tran, Radu Soricut, Anikait Singh, Jaspiar Singh, Pierre Sermanet, Pannag R. Sanketi, Grecia Salazar, Michael S. Ryoo, Krista Reymann, Kanishka Rao, Karl Pertsch, Igor Mordatch, Henryk Michalewski, Yao Lu, Sergey Levine, Lisa Lee, Tsang-Wei Edward Lee, Isabel Leal, Yuheng Kuang, Dmitry Kalashnikov, Ryan Julian, Nikhil J. Joshi, Alex Irpan, Brian Ichter, Jasmine Hsu, Alexander Herzog, Karol Hausman, Keerthana Gopalakrishnan, Chuyuan Fu, Pete Florence, Chelsea Finn, Kumar Avinava Dubey, Danny Driess, Tianli Ding, Krzysztof Marcin Choromanski, Xi Chen, Yevgen Chebotar, Justice Carbajal, Noah Brown, Anthony Brohan, Montserrat Gonzalez Arenas, and Kehang Han. RT-2: vision-language-action models transfer web knowledge to robotic control. In *Conference on Robot Learning (CoRL)*, volume 229, pp. 2165–2183. PMLR, 2023.

## A ADDITIONAL IMPLEMENTATION DETAILS

### A.1 HEURISTICS FOR SUB-GOAL KEYPOSE DISCOVERY

Building on keypose discovery (James & Davison, 2022), we propose the Sub-goal Keypose Discovery method to identify sub-goal keyposes from demonstrations, focusing on changes in the gripper’s state and touch forces. This is particularly relevant for object manipulation tasks, where the robot’s interactions with objects can be segmented into discrete sub-goals.

The implementation of the Sub-goal Keypose Discovery algorithm starts with a set of pre-computed keyposes, which are frames selected from the demonstration sequence through an initial keypose discovery process. We introduce two functions: `touch_change`, shown in Algorithm 2, and `gripper_change`, shown in Algorithm 3, to evaluate whether a keypose qualifies as a sub-goal. The first function checks for significant changes in the gripper’s touch forces, while the second evaluates changes in the gripper’s open/close state. The pseudocode in Algorithm 4 outlines the heuristic steps for identifying sub-goal keyposes.

One current limitation of the Sub-goal Keypose Discovery method is its inability to effectively handle tasks involving tool use, which we plan to address in future research.

---

#### Algorithm 2: touch\_change Function

---

**Input:** Demonstration sequence *demo*, Keypose index *k*, Threshold *touch\_threshold*, Tolerance *delta*

**Output:** Boolean indicating significant touch force change

**begin**

    Set *start* to  $\max(0, k - \text{touch\_threshold})$ ;

**for** each index *j* from *start* to *k-1* **do**

**if** Touch forces at *j* differ from Touch forces at *k* within tolerance *delta* **then**

**return** *True*;

**return** *False*;

---



---

#### Algorithm 3: gripper\_change Function

---

**Input:** Demonstration sequence *demo*, Keypose index *k*, Threshold *gripper\_threshold*

**Output:** Boolean indicating gripper state change

**begin**

    Set *start* to  $\max(0, k - \text{gripper\_threshold})$ ;

**for** each index *j* from *start* to *k-1* **do**

**if** Gripper state at *j* differs from Gripper state at *k* **then**

**return** *True*;

**return** *False*;

---

### A.2 DETAILS OF GRAVMAP SYNTHESIS

#### A.2.1 TRAINING PHASE

To facilitate GravMap synthesis, we assign a goal action to each keypose by linking it to the action performed at the nearest future sub-goal. This association enables us to determine the relevant cost and gripper state for different regions of the GravMap. In the first map,  $m_c \in \mathbb{R}^{w \times h \times d}$ , the cost is lower near the positions of the robotic end-effector at these sub-goal keyposes and higher as the distance increases. In the second map,  $m_o \in \mathbb{R}^{w \times h \times d}$ , areas near the end-effector’s position at the sub-goal keyposes reflect the gripper state at the sub-goal, while other areas reflect the gripper state at the current frame.

**Algorithm 4:** Heuristics for Sub-goal Keypose Discovery

**Input:** Demonstration sequence  $demo$ , Task type  $task\_str$ , Threshold parameters  $touch\_threshold$ ,  $gripper\_threshold$ ,  $delta$

**Output:** List of sub-goal keyposes  $sub\_goal\_keyposes$

**begin**

```

Initialize  $sub\_goal\_keyposes$  as an empty list;
Identify keyposes from  $demo$  using keypose discovery method;
for each keypose  $k$  in keyposes do
  if  $task\_str$  is a task involving touch without grasping then
    if  $touch\_change(demo, k, touch\_threshold, delta)$  then
      Append  $k$  to  $sub\_goal\_keyposes$ ;
    else
      if  $gripper\_change(demo, k, gripper\_threshold)$  or  $touch\_change(demo, k,$ 
         $touch\_threshold, delta)$  then
        Append  $k$  to  $sub\_goal\_keyposes$ ;
  Append the last keypose to  $sub\_goal\_keyposes$ ;
return  $sub\_goal\_keyposes$ ;

```

**Algorithm 5:** GravMap Generation

**Input:** Instruction  $\ell$ , Observed RGB Image  $\mathcal{O}$

**Prompt:** Prompt for Detector  $\mathcal{P}_{det}$ , Prompt for Planner  $\mathcal{P}_{plan}$ , Prompt for Composer  $\mathcal{P}_{com}$ ,  
 Few-shot task specified prompt  $\mathcal{P}_{task} = \{\mathcal{P}'_{det}, \mathcal{P}'_{plan}, \mathcal{P}'_{com}\}$ , Cost Map Prompt  $\mathcal{P}_{cost}$ ,  
 Gripper Map Prompt  $\mathcal{P}_{gripper}$

**Output:** GravMap  $m$

**begin**

```

 $\mathcal{O}' \leftarrow \text{Semantic-SAM}(\mathcal{O});$  // Label objects with numerical tags
 $\mathcal{C} \leftarrow \text{Detector}(\ell, \mathcal{O}', \mathcal{P}_{det}, \mathcal{P}'_{det});$  // Select relevant objects and get
  corresponding 3D positions as context
 $ST \leftarrow \text{Planner}(\ell, \mathcal{C}, \mathcal{P}_{plan}, \mathcal{P}'_{plan});$  // Infer sub-tasks  $ST = (st_1, st_2, \dots, st_i)$ 
Function calls, parameters  $\leftarrow \text{Composer}(ST, \mathcal{C}, \mathcal{P}_{com}, \mathcal{P}'_{com});$  // Generate API
  calls and their parameters for generating  $g^{pos}$  and  $g^{open}$ 
 $g^{pos} \leftarrow \text{get\_cost\_map}(\text{Function calls, parameters}, \mathcal{P}_{cost});$ 
 $g^{open} \leftarrow \text{get\_gripper\_map}(\text{Function calls, parameters}, \mathcal{P}_{gripper});$ 
 $m \leftarrow \text{GravMap generator}(\text{cat}(g^{pos}, g^{open}));$ 
return  $m$ ;

```

## A.2.2 INFERENCE PHASE

In this section, we introduce the complete pipeline for GravMap generation, as outlined in Algorithm 5. This includes Algorithm 1, which details the process of generating a GravMap from a language instruction  $\ell$  and an observed RGB image  $\mathcal{O}$ . The GravMap generation pipeline integrates VLMs to interpret instructions, ground them in the visual context, and translate them into coarse 3D voxel representations, i.e., the GravMap.

Our pipeline consists of the following three components:

- **Detector.** Starting with an instruction  $\ell$  and an observed RGB image  $\mathcal{O}$ , the RGB image is passed through the Semantic-SAM segmentation model, which labels each object with a numerical tag, producing a labeled image  $\mathcal{O}'$ . The GPT4o-based Detector uses the prompts  $\mathcal{P}_{det}$  and  $\mathcal{P}'_{det}$  (adapted from Huang et al. (2024)) to select relevant objects and obtain their 3D positions. The output is a set of selected objects, or context  $\mathcal{C}$ , which includes the objects' identities and their spatial coordinates in the 3D environment. In the VLM setting, the Detector accesses initial RGB images from four views: wrist, left shoulder, right shoulder,

and front camera. In the manual setting, precise 3D object attributes are provided from the simulation.

- **Planner.** The GPT4o-based Planner takes the instruction  $\ell$ , context  $\mathcal{C}$ , and planner-specific prompts  $\mathcal{P}_{\text{plan}}$  and  $\mathcal{P}'_{\text{plan}}$  (adapted from Huang et al. (2023)) to infer a sequence of sub-tasks  $(st_1, st_2, \dots, st_i)$ . Each sub-task describes an action or interaction needed to fulfill the instruction  $\ell$ . Progress is tracked based on the robot’s gripper state (open/closed) and whether it is holding an object. The current sub-task is then passed to the Composer for further processing.
- **Composer.** Following Huang et al. (2023), the GPT4o-based Composer parses each inferred sub-task  $st_i$  using corresponding prompts  $\mathcal{P}_{\text{com}}$  and  $\mathcal{P}'_{\text{com}}$ . The Composer generates the sub-goal position  $g^{\text{pos}}$  and sub-goal openness  $g^{\text{open}}$  by recursively generating code. This includes calls to `get_cost_map` and `get_gripper_map`, which are triggered by cost map prompt  $\mathcal{P}_{\text{cost}}$  and gripper map prompt  $\mathcal{P}_{\text{gripper}}$ . For example, for a sub-task like “push close the topmost drawer,” the Composer might generate: `get_cost_map('a point 30cm into the topmost drawer handle')` and `get_gripper_map('close everywhere')`. Natural language parameters are parsed by GPT to generate code that assigns values to  $g^{\text{pos}}$  and  $g^{\text{open}}$ . The final GravMap generator in Algorithm 1 then processes  $g^{\text{pos}}$  and  $g^{\text{open}}$  to generate the GravMap  $m$ .

The prompts mentioned above can be found on the website: <https://gravmad.github.io>.

### A.3 DETAIL OF MODEL ARCHITECTURE AND HYPER-PARAMETERS FOR GRAVMAD

The detailed hyperparameters of GravMAD are listed in Table 3. Additionally, Fig. 5 provides a detailed overview of GravMAD’s modules, including the 3D Scene Encoder and the prediction heads.

(a) The 3D Scene Encoder processes visual and language information separately, merging them via a cross-attention mechanism, with proprioception integrated through FiLM. This allows the model to understand tasks like “Take the chicken off the grill” in a 3D environment. First, the visual input is processed by a 2D Visual Encoder, transforming image data into feature representations. These 2D features are then passed through a 3D lifting module, converting them into 3D representations using depth information. Simultaneously, the language input, such as the instruction “Take the chicken off the grill”, is encoded into language tokens by the Language Encoder. Finally, the 3D visual features and language tokens are combined through cross-attention, producing 3D Scene tokens.

(b) Each prediction head consists of Attention layers and an MLP. The Auxiliary Position Head receives tokens from the previous layer, which first go through cross-attention with GravMap tokens, followed by self-attention to refine the features. The tokens are then passed through an MLP to output the sub-goal end-effector position. Similarly, the Auxiliary Openness Head takes tokens from the self-attention layer of the Auxiliary Position Head and uses an MLP to predict the sub-goal gripper openness. The Position Head follows the same process as the Auxiliary Position Head, while the Openness Head mirrors the Auxiliary Openness Head. The Rotation Head processes tokens with self-attention and an MLP to predict rotation error.

### A.4 COMPARISON BETWEEN GRAVMAD AND OTHER BASELINE MODELS

We compare GravMAD with Voxposer (Huang et al., 2023) and 3D Diffuser Actor (Ke et al., 2024) in Fig. 6.

(a) **Voxposer.** We describe our reproduction of Voxposer on RLBench. Voxposer uses our SOM-driven Detector to process the input observation and instruction, generating context information. The Planner then receives this context and outputs a sub-goal, representing an intermediate step necessary for the overall motion plan. The Composer processes this sub-goal, producing three maps: Cost Map, Rotation Map, and Gripper Map. These maps guide the robot’s movement toward the target in the environment. Note that Voxposer’s testing process involves a different number of steps compared to 3D Diffuser Actor and GravMAD, completing only after all LLM inferences are executed.

(b) **3D Diffuser Actor.** We use the language-enhanced version of 3D Diffuser Actor as a baseline. 3D Diffuser employs a 3D Scene Encoder to transform visual and language inputs into 3D Scene

	Values
<b>Sub-goal Keypose Discovery</b>	
touch_threshold	2
Tolerance: delta	0.005
gripper_threshold	4
<b>GravMap</b>	
map_size: $S_m$	100
offset_range: $\beta_o$	3
radius: $\beta_r$	3
downsample ratio: $\beta_d$	4
number of sampled points: $N_p$	1024
<b>Model</b>	
image_size	256
token_dim	120
diffusion_timestep	100
noise_scheduler: position	scaled_linear
noise_scheduler: rotation	squaredcos
action_space	absolute pose
<b>Train</b>	
batch_size	8
optimizer	Adam
train_iters	600K
learning_rate	$1e^{-4}$
weight_decay	$5e^{-4}$
loss weight: $\omega_1$	30
loss weight: $\omega_2$	10
loss weight: $\omega_3$	30
loss weight: $\omega_4$	10
<b>Evaluation</b>	
maximal step except push_button_light	25
maximal step of push_button_light	3

Table 3: **Hyper-parameters for GravMAD**, including Sub-goal Keypose Discovery, GravMap, model configuration, training, and evaluation.

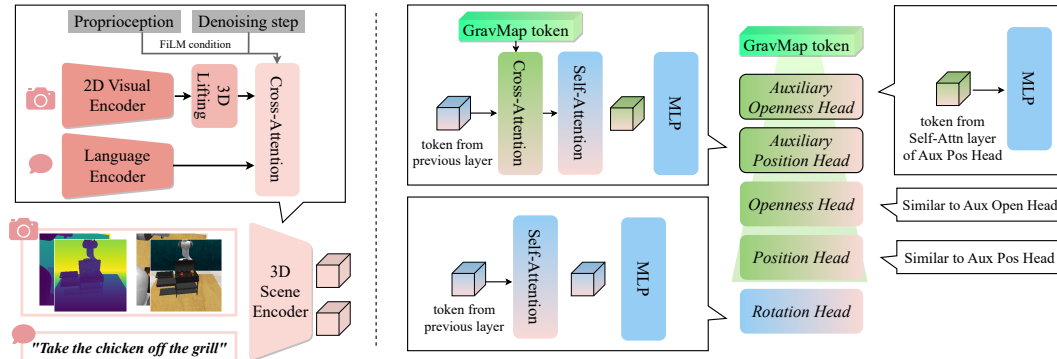


Figure 5: **Detailed description of the modules in GravMAD**, including the 3D Scene Encoder and the prediction heads

tokens, providing an understanding of the 3D environment. An MLP encodes noisy estimates of position and rotation into corresponding tokens, which are then fed, along with the 3D Scene tokens, into a denoising network for action diffusion. This network, conditioned on proprioception and the denoising step, includes attention layers, Openness Head, Position Head, and Rotation Head. During diffusion, noisy position/rotation tokens attend to 3D Scene tokens, and cross-attention with instruction tokens enhances language understanding. These instruction tokens are also used in the prediction processes of the Openness, Position, and Rotation heads.

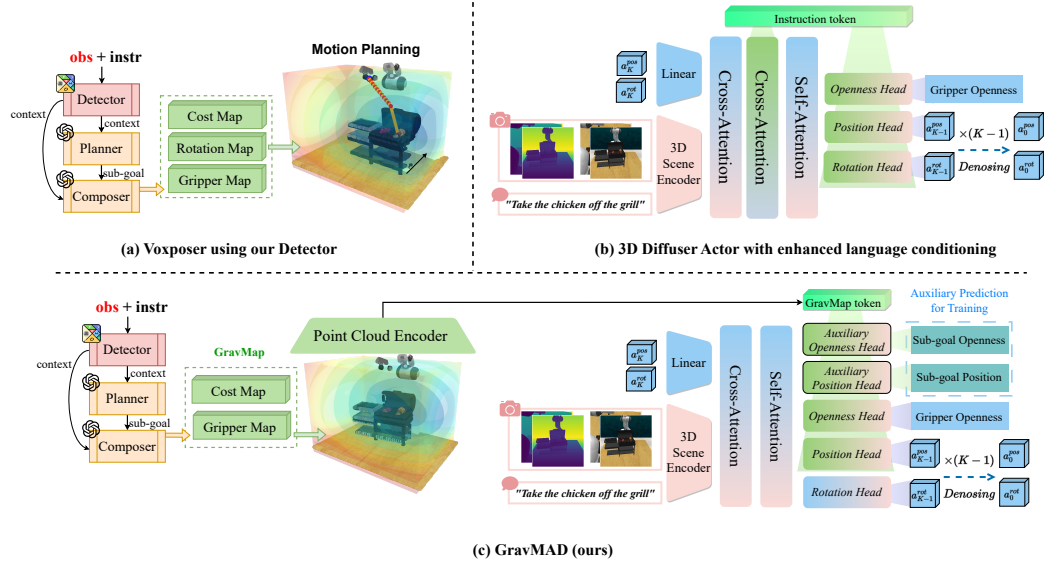


Figure 6: **Comparison of GravMAD with Voxposer and 3D Diffuser Actor.** Unlike Voxposer, which uses planning, GravMAD leverages GravMaps for learning. Compared to 3D Diffuser Actor, GravMAD employs GravMap tokens to guide the action diffusion process and introduces auxiliary position and openness heads to improve representation learning.

(c) **GravMAD (ours).** GravMAD shares components with Voxposer, such as the Detector, Planner, and Composer, but incorporates task-specific prompt engineering. Unlike Voxposer, which uses maps for planning, GravMAD encodes these maps into tokens using a point cloud encoder, which are then employed in the action diffusion process. Compared to 3D Diffuser Actor, the key difference is that GravMAD uses GravMap tokens instead of language tokens, improving generalization. Additionally, GravMAD introduces two auxiliary tasks to predict sub-goals, enhancing representation learning.

## B ADDITIONAL EXPERIMENTAL DETAILS

### B.1 BASE TASK

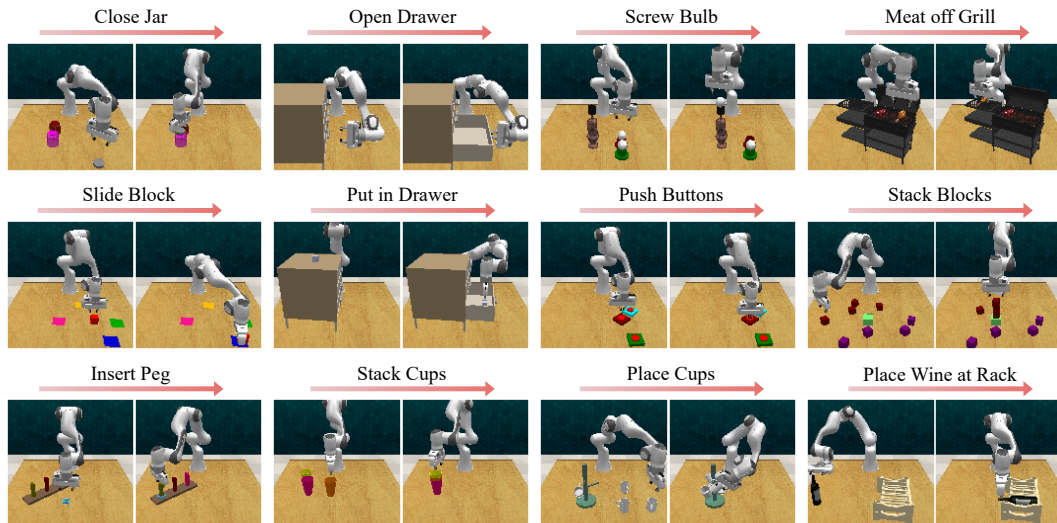


Figure 7: Visualization of 12 base tasks.

Table 4: The 12 base tasks selected from RL Bench (James et al., 2020a)

Task	Variation Type	# of Variations	Avg. Keyposes	Language Template
close jar	color	20	6.0	“close the — jar”
open drawer	placement	3	3.0	“open the — drawer”
screw bulb	color	20	7.0	“screw in the — light bulb”
meat off grill	category	2	5.0	“take the — off the grill”
slide block	color	4	4.7	“slide the block to — target”
put in drawer	placement	3	12.0	“put the item in the — drawer”
push buttons	color	50	3.8	“push the — button, [then the — button]”
stack blocks	color, count	60	14.6	“stack — — blocks”
insert peg	color	20	5.0	“put the ring on the — spoke”
stack cups	color	20	10.0	“stack the other cups on top of the — cup”
place cups	count	3	11.5	“place — cups on the cup holder”
place wine	count	3	5.0	“stack the wine bottle to the — of the rack”

As shown in Fig. 7, we select 12 tasks from RL Bench (James et al., 2020a), each containing 2 to 60 variants in the instructions, covering differences in color, placement, category, and count. In addition to instruction variations, the objects, distractors, and their positions and scenes are randomly initialized in the environment. The templates representing task goals in the instructions are also modified while maintaining their semantic meaning. A summary of the 12 tasks is provided in Table 4.

We provide a detailed description of each task below and explain modifications from RL Bench origin codebase.

#### B.1.1 CLOSE JAR

**Task:** Close the jar by placing the lid on the jar.

**filename:** close\_jar.py

**Modified:** The modified success condition registers a single DetectedCondition to check if the jar lid is correctly placed on the jar using a proximity sensor, discarding the previous condition of checking if nothing is grasped by the gripper.

**Success Metric:** The jar lid is successfully placed on the jar as detected by the proximity sensor.

#### B.1.2 OPEN DRAWER

**Task:** Open the drawer by gripping the handle and pulling it open.

**filename:** open\_drawer.py

**Modified:** The cam\_over\_shoulder\_left camera’s position and orientation were modified to better observe the drawer. The camera was repositioned to [0.2, 0.90, 1.10] and reoriented to [0.5\* $\pi$ , 0, 0].

**Success Metric:** The drawer is successfully opened to the desired position as detected by the joint condition on the drawer’s joint.

#### B.1.3 SCREW BULB

**Task:** Screw in the light bulb by picking it up from the holder and placing it into the lamp.

**filename:** light\_bulb\_in.py

**Modified:** No.

**Success Metric:** The light bulb is successfully screwed into the lamp and detected by the proximity sensor.

#### B.1.4 MEAT OFF GRILL

**Task:** Take the specified meat off the grill and place it next to the grill.

**filename:** meat\_off\_grill.py

**Modified:** The cam\_over\_shoulder\_right camera’s position and orientation were modified to better observe the drawer. The camera was repositioned to [0.20,-0.36,1.85] and reoriented to [-0.85\* $\pi$ , 0,  $\pi$ ].

**Success Metric:** The specified meat is successfully removed from the grill and detected by the proximity sensor.

#### B.1.5 SLIDE BLOCK

**Task:** Slide the block to the target of a specified color.

**filename:** slide\_block\_to\_color\_target.py

**Modified:** No.

**Success Metric:** The block is successfully detected on top of the target color as indicated by the proximity sensor.

#### B.1.6 PUT IN DRAWER

**Task:** Put the item in the specified drawer.

**filename:** put\_item\_in\_drawer.py

**Modified:** The `cam_over_shoulder_left` camera's position and orientation were modified to better observe the drawer. The camera was repositioned to [0.2, 0.90, 1.15] and reoriented to [0.5\* $\pi$ , 0, 0].

**Success Metric:** The item is successfully placed in the drawer as detected by the proximity sensor.

#### B.1.7 PUSH BUTTONS

**Task:** Press the buttons of the specified color in order

**filename:** push\_buttons.py

**Modified:** No.

**Success Metric:** The buttons are successfully pushed in order.

#### B.1.8 STACK BLOCKS

**Task:** Stack a specified number of blocks of the same color in a vertical stack.

**filename:** stack\_blocks.py

**Modified:** No.

**Success Metric:** The blocks are successfully stacked according to the specified color and number.

#### B.1.9 INSERT PEG

**Task:** Insert a square ring onto the spoke with the specified color.

**filename:** insert\_onto\_square\_peg.py

**Modified:** No.

**Success Metric:** The square ring is successfully placed onto the correctly colored spoke.

#### B.1.10 STACK CUPS

**Task:** Stack two cups on top of the cup with the specified color.

**filename:** stack\_cups.py

**Modified:** No.

**Success Metric:** The cups are successfully stacked with the correct cup as the base.

#### B.1.11 PLACE CUPS

**Task:** Place a specified number of cups onto a cup holder.

**filename:** place\_cups.py

**Modified:** No.

**Success Metric:** The cups are successfully placed onto the holder according to the task instructions.

#### B.1.12 PLACE WINE AT RACK LOCATION

**Task:** Place the wine bottle onto the specified location on the wine rack.

**filename:** place\_wine\_at\_rack\_location.py

**Modified:** No.

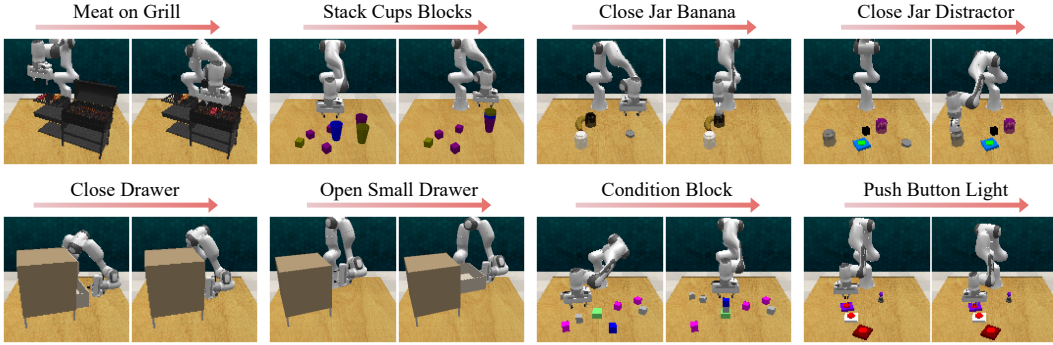


Figure 8: Visualization of 8 novel tasks.

Table 5: The 8 novel tasks changed based on base tasks.

Task	Variation Type	# of Variations	Avg. Keyposes	Language Template
close drawer	placement	3	2.0	"close the — drawer"
close jar banana	placement	2	6.0	"close the jar closer to the banana"
close jar distractors	color	20	6.0	"close the — jar"
condition block	color, count	72	11.0	"build a tall tower out of — — cubes, and add a blue block if it exists"
meat on grill	category	2	5.0	"put the — on the grill"
open small drawer	placement	3	3.0	"open the — drawer"
stack cups blocks	color	20	10.0	"Identify the most common color in the block pile, and stack the other cups on the cup that matches that color"
push button light	color	20	2.0	"push the button with the same color as the light"

**Success Metric:** The wine bottle is successfully placed at the correct rack location and released from the gripper.

## B.2 NOVEL TASK

As shown in Fig. 8, we create 8 novel tasks that differ from the original training tasks to test policy generalization. These tasks feature scenes and objects similar to those in the training tasks. A summary of the seven tasks is provided in Table 5.

We provide a detailed description of each novel task below and explain the modifications from the base tasks.

### B.2.1 MEAT ON GRILL

**Task:** Place either a chicken or a steak on the grill depending on the variation.

**filename:** meat\_on\_grill.py

**Base task:** meat off grill.

**Modified:** The task requires placing meat onto the grill, whereas the base task involves removing it. The `cam_over_shoulders_right` camera’s position and orientation were modified to better observe the drawer. The camera was repositioned to  $[0.20, -0.36, 1.85]$  and reoriented to  $[-0.85 * \text{math.pi}, 0, \text{math.pi}]$ .

**Success Metric:** The selected meat (chicken or steak) is successfully placed on the grill and released from the gripper.

### B.2.2 STACK CUPS BLOCKS

**Task:** Identify the most common color in the block pile, and stack the other cups on the cup that matches that color.

**filename:** stack\_cups\_blocks.py

**Base task:** Stack cups.

**Modified:** The task involves identifying the cup that matches the most common color among the distractor blocks, then stacking the other two cups on top. The base task is simply stacking the cups without considering block colors.

**Success Metric:** Success is measured when the correct cup is stacked with the other cups based on the color identification and all cups are within the target area defined by the proximity sensor.

### B.2.3 CLOSE JAR BANANA

**Task:** Close the jar that is closer to the banana by screwing on its lid.

**filename:** close\_jar\_banana.py

**Base task:** close jar.

**Modified:** The task involves identifying the jar closer to the banana and screwing its lid on, while the base task only requires closing a jar without proximity consideration.

**Success Metric:** The lid is successfully placed on the jar closest to the banana, confirmed by the proximity sensor.

### B.2.4 CLOSE JAR DISTRACTOR

**Task:** Close the jar by screwing on the lid, while distractor objects are present.

**filename:** close\_jar\_distractor.py

**Base task:** close jar.

**Modified:** The task includes distractor objects, such as a button and block, which are colored and placed near the jars. These objects have been encountered during training, adding complexity compared to the base task.

**Success Metric:** The jar lid is successfully placed on the target jar, confirmed by the proximity sensor.

### B.2.5 CLOSE DRAWER

**Task:** Close one of the drawers (bottom, middle, or top) by sliding it shut.

**filename:** close\_drawer.py

**Base task:** open drawer.

**Modified:** The task involves closing the drawer instead of opening it.

**Success Metric:** The selected drawer is closed successfully, confirmed by the joint position of the drawer.

### B.2.6 OPEN DRAWER SMALL

**Task:** Open one of the smaller drawers (bottom, middle, or top) by sliding it open.

**filename:** open\_drawer\_small.py

**Base task:** open drawer.

**Modified:** The task involves opening a smaller drawer compared to the base task, with adjusted camera settings for better visibility.

**Success Metric:** The selected drawer is opened successfully, verified by the joint position of the drawer.

### B.2.7 CONDITION BLOCK

**Task:** Stack a specified number of blocks and, if the blue block is present, add it to the stack.

**filename:** condition\_block.py

**Base task:** stack blocks.

**Modified:** The task involves stacking a specified number of blocks, with an additional requirement to include the blue block if it is present.

**Success Metric:** The correct number of target blocks are stacked, and if the blue block is present, it is also correctly added to the stack.

### B.2.8 PUSH BUTTON LIGHT

**Task:** Push the button that matches the color of a light bulb on the first attempt.

**filename:** push\_buttons\_light.py

**Base task:** push button.

**Modified:** The task involves pressing a single button that matches the color of a light bulb. The

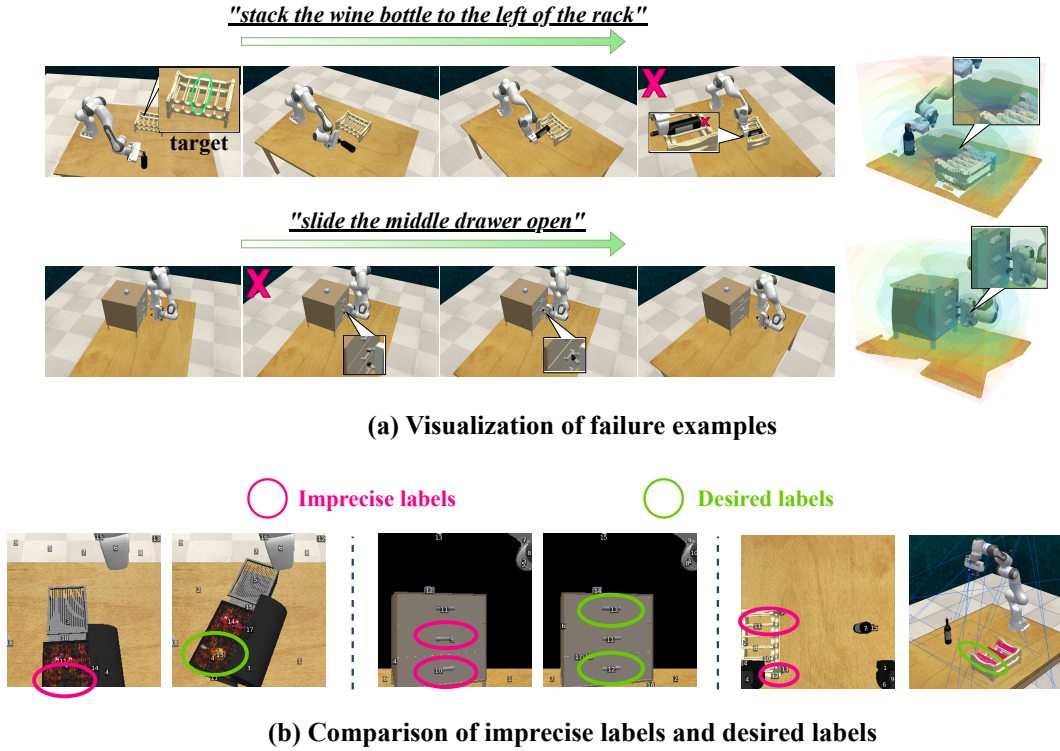


Figure 9: **Failure cause analysis**, including (a) visualization of failure examples; (b) comparison of imprecise labels and expected labels.

button must be pressed correctly on the first attempt; repeated attempts are not allowed.

**Success Metric:** The correct button matching the light bulb’s color is pressed on the first attempt.

### B.3 FAILURE CASES OF GRAVMAD

In this section, we analyze why GravMAD underperforms compared to the baseline model 3D Diffuser Actor on certain base tasks, particularly in the “Place Wine” task and drawer-related tasks.

As discussed in the main paper, GravMaps represent spatial relationships in 3D space, but this introduces a challenge: areas close to the sub-goal often share the same cost value, as seen in the value map on the right side of Fig. 9 (a). This uniform cost value can mislead the robot into assuming it should complete the sub-goal within that area. For tasks requiring precise actions, such as the “Open Drawer” task, GravMaps’ coarse guidance may lead to suboptimal performance compared to 3D Diffuser Actor. In the left schematic of Fig. 9(a), the robot must grasp the center of a small handle to achieve optimal performance in the “Open Drawer” task. This high precision demand on the end-effector results in a lower success rate for GravMAD. This limitation extends to the “Put in Drawer” task, which depends on the successful completion of “Open Drawer”. Similarly, in the “Place Wine” task, insufficient predictive accuracy causes the robot to misalign the bottle with the correct slot by one unit, leading to failure.

In the VLM setting, sub-goal accuracy often suffers, as shown in Fig. 9(b), further reducing model performance. These inaccuracies typically arise from two factors: (1) SAM may fail to accurately identify ideal areas, leading to imprecise contextual information from the Detector module for tasks like “Place Wine”, “Open Drawer”, and “Put in Drawer”; (2) the camera’s positioning may not capture the full scene, leaving some task-relevant objects out of view, as seen in tasks like “Meat off Grill”. To overcome these VLM limitations, potential solutions include: (1) integrating multi-view information into the Detector for a more comprehensive scene observation; and (2) using a more granular segmentation model to provide GPT-4 with a wider range of labels, improving the quality of the context generated by the Detector.